PAPER

Tailoring interactions of carbon and sulfur in Li–S battery cathodes: significant effects of carbon–heteroatom bonds†

Xia Li,[a] Xifei Li,[a] Mohammad N. Banis,[a] Biqiong Wang,[ab] Andrew Lushington,[a] Xiaoyu Cui,[c] Ruying Li,[a] Tsun-Kong Sham[b] and Xueliang Sun*[a]

In this study, effects of carbon–heteroatom bonds on sulfur cathodes were investigated. A series of carbon black substrates were prepared using various treatments to introduce nitrogen or oxygen surface species. Our results indicated that nitrogen-doped carbon black significantly improved the electrochemical performance of sulfur cathode materials. Synchrotron-based XPS revealed that the defect sites of nitrogen-doped carbon are favorable for the discharge product deposition, leading to a high utilization and reversibility of sulfur cathodes. Our studies also found that the introduction of oxygen functional groups results in deteriorated performance of Li–sulfur batteries due to the reduced conductivity and unwanted side reactions occurring between sulfur and surface oxygen species.

Introduction

Recently, Li–sulfur batteries have been considered as powerful energy storage systems that can be utilized in electric vehicles.[1] Associated with its light atomic weight and potential multiple-electron reaction, sulfur as a cathode material endows an overwhelmingly high theoretical capacity and energy density.[2–4] Furthermore, sulfur is an abundant and environmentally benign element with low production costs, making Li–sulfur batteries competitive candidates for next generation battery systems. However, two main issues impede the practical application of Li–sulfur batteries.[2–4] The first is the inherent insulating nature of sulfur and lithium sulfide, resulting in limited performance of Li–sulfur batteries.[1–3,5] Secondly, dissolved polysulfides migrate between the cathode and anode, called the "shuttle effect", and participate in unexpected side reactions, resulting in lithium metal corrosion and drastic loss of the sulfur active material.[5–8]

To address these issues, carbon nanomaterials have been applied as sulfur cathodes due to their high conductivity, high pore volume and fitted pore size, such as mesoporous carbon black, one dimensional carbon nanofibers and nanotubes, and two dimensional graphene.[9–11] Recently, carbon materials used for sulfur cathodes have also been extended by introducing heteroatoms into the carbon matrix.[12–17] Wang et al.[14] revealed that the introduction of nitrogen enhanced the chemical adsorption between sulfur and oxygen species of carbon. Archer et al.[13] stated that the Li–N interaction is responsible for uniform Li_2S deposition on nitrogen-enriched polymers, leading to improved electrochemical performance of Li_2S based cathode materials. These research studies demonstrated that carbon–heteroatom bonds alter the electrochemical performance of sulfur cathodes. However, the effects of other heteroatoms, such as oxygen, embedded into the carbon matrix have not been extensively explored.
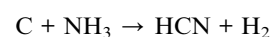
In this paper, various treatments are employed on commercial carbon black to introduce nitrogen and oxygen heteroatoms. The treated carbon black has comparable physical properties (surface area, pore size, and pore volume), and serves as a good system towards isolating the effect of heteroatoms on the performance of sulfur cathodes. In-depth discussion by synchrotron-based XPS was carried out to reveal electrochemical mechanisms.

Experimental

Preparation of carbon black

Commercial carbon black N330 was chosen as a starting material. Nitrogen inclusion was carried out by pyrolyzing 500 mg of carbon black powder under NH_3 at 1050 °C for 3–5 minutes, yielding a highly porous structure.

Previous reports have indicated that NH_3 reacts with carbon black with the following reaction mechanism:[18]
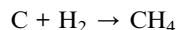
$$C + NH_3 \rightarrow HCN + H_2$$

[a]Department of Mechanical and Materials Engineering, University of Western Ontario, London, ON, Canada N6A 5B9. E-mail: xsun@eng.uwo.ca; Fax: +1 519 661 3020; Tel: +1 519 661 2111 ext. 87759
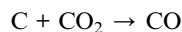
[b]Department of Chemistry, University of Western Ontario, London, Ontario, N6A 5B7 Canada

[c]Canadian Light Source, Saskatoon, SK, S7N 2V3, Canada

$$C + H_2 \rightarrow CH_4$$

Oxygen species were introduced into N330 in a similar procedure with the use of CO_2 gas. The reaction occurs in the following manner:[19]

$$C + CO_2 \rightarrow CO$$

The oxygenated sample was then further pyrolysed under H_2 at 950 °C to remove oxygen-bearing functional groups. Herein, carbon black samples treated under NH_3, CO_2, and CO_2/H_2 are named as N-N330, O-N330, and RO-N330, respectively.

Preparation of sulfur–carbon black composites

As-prepared carbon black materials were mixed with pristine sulfur and dried at 80 °C over 12 h to remove moisture. The sulfur–carbon black mixture was transferred to a sealed steel reactor and heated at 150 °C over 9 h and then 300 °C over 3 h. The obtained sulfur–carbon black composites had a sulfur loading of 60 ± 2 wt% and were confirmed by thermogravimetric analysis (TGA). Sulfur–carbon black composites are termed as S/N-N330, S/O-N330, and S/RO-N330, respectively.

Physical characterization

Morphological observations were characterized using a Hitachi S-4800 field emission scanning electron microscope (FE-SEM) operating at 5 keV. TGA was carried out on a TA SDT Q600 in a N_2 atmosphere from room temperature to 700 °C at a rate of 10 °C min^{-1}. N_2 adsorption/desorption isotherms of carbon black materials were collected using a Folio Micromeritics TriStar II Surface Area and Pore Size Analyser. X-ray photoelectron spectroscopy (XPS) was conducted using a Kratos Axis Ultra Al α unit. Raman scattering (RS) spectra was obtained using a HORIBA Scientific LabRAM HR Raman spectrometer system equipped with a 532.4 nm laser. Fourier transform-infrared (FTIR) measurements were determined by the KBr method with a Nicolet 6700 FT-IR recorded in the transmittance mode over a range of 400–4000 cm^{-1} by averaging 40 scans with a resolution of 8 cm^{-1}. Synchrotron-based XPS was conducted on the variable line spacing plane grating monochromator (VLS PGM) beamline at the Canadian Light Source (CLS), located at the University of Saskatchewan in Saskatoon.[20]

Electrochemical characterization

CR-2032 type coin cells were assembled in an argon filled glove box. Assembled batteries were made using Li metal as an anode, a polypropylene separator, and the as-prepared electrode as the cathode. 1 M LiTFSI salt dissolved in dioxolane (DOL):dimethoxyethane (DME) in a 1 : 1 volume ratio was used as the electrolyte. The electrodes were prepared by slurry casting on aluminum foil as a current collector. The slurry mass ratio of the active material, acetylene black, and polyvinylidene fluoride (PVDF) was 7 : 2 : 1. The as-prepared electrodes were dried at 80 °C over 12 h under vacuum. Cyclic voltammetry (CV) was performed on a versatile multichannel potentiostation 3/Z (VMP3) under a scanning rate of 0.1 mV s^{-1} between 1.0 V and 3.0 V (vs. Li/Li$^+$). Charge–discharge characteristics were galvanostatically tested in the range of 1.0 V–3.0 V (vs. Li/Li$^+$) at room temperature using an Arbin BT-2000 Battery Tester.

Results and discussion

Previous research has indicated that the physical surface properties (morphology, surface area, pore volume, and pore
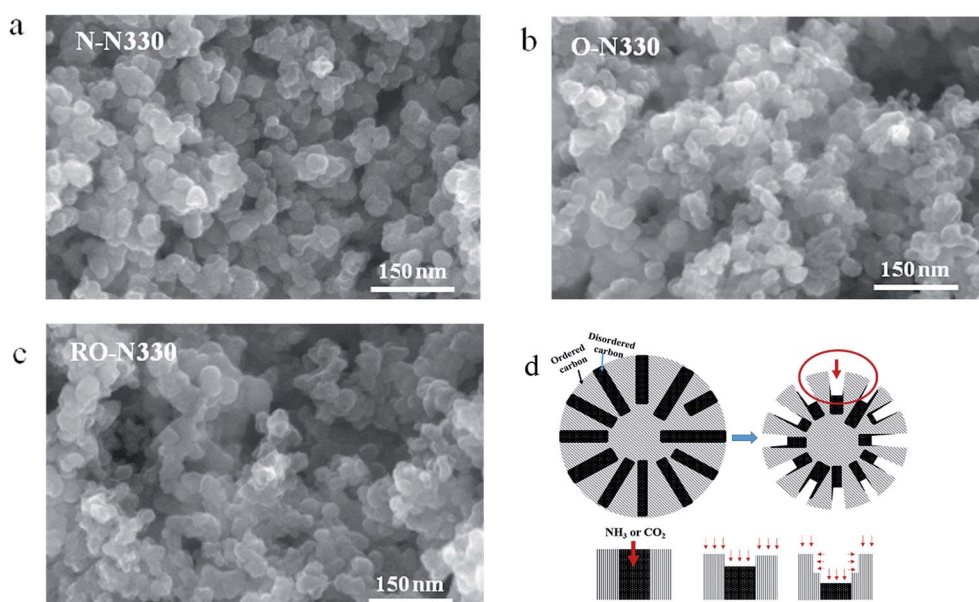

Fig. 1 FE-SEM images of carbon black (a) N-N330, (b) O-N330, and (c) RO-N330 and schematic of (d) porous structure formation of as-prepared carbon black samples.

This journal is © The Royal Society of Chemistry 2014

J. Mater. Chem. A, 2014, 2, 12866–12872 | 12867

size) of carbon materials have significant influence on the performance of sulfur cathodes.[2–4] In order to isolate the role of heteroatoms in Li–S battery systems, carbon materials with similar physical surface properties but different heteroatoms need to be used. Fig. 1 shows FE-SEM images of as-prepared carbon black materials. Morphologies across all three samples indicate that nanoparticles are agglomerated and are within 30–50 nm. As shown in Table 1, as-prepared carbon black materials have comparable physical surface properties with surface areas between 1200 and 1300 $m^2 g^{-1}$; pore volumes in the range of 1.15–1.25 $cm^3 g^{-1}$; and a mean pore size between 3 and 4 nm. The mechanism of porous structure formation has been well

described previously by Jaouen et al.[18,19,21] Pristine carbon black N330 is a spherical carbon particle without pores, consisting of disordered carbon and graphitic carbon (Fig. 1d). During the heteroatom doping process, NH_3 or CO_2 is proposed to react with both graphitic and disordered carbon but at different reaction rates, resulting in the formation of the porous structure for carbon black. With the carbon black consumed, micropores increase in size, producing a mesoporous structure.[18,19] Pore formation is conducted in a similar manner under different atmospheric conditions (CO_2 or NH_3), and thereby the three carbon black materials are comparable in physical surface properties.

The XPS survey spectrum of N-N330 confirms the introduction of nitrogen (N doped or N functional groups) into carbon black with a concentration of 1.5 at%, as shown in Fig. S1.† FTIR spectra (Fig. S2†) of O-N330 display C–O related vibrations appearing at 1470 cm^{-1} and 720 cm^{-1}, demonstrating the successful introduction of oxygen-bearing functional groups.[22,23] Based on the above results, we have successfully

Table 1 Physical surface properties of carbon black samples

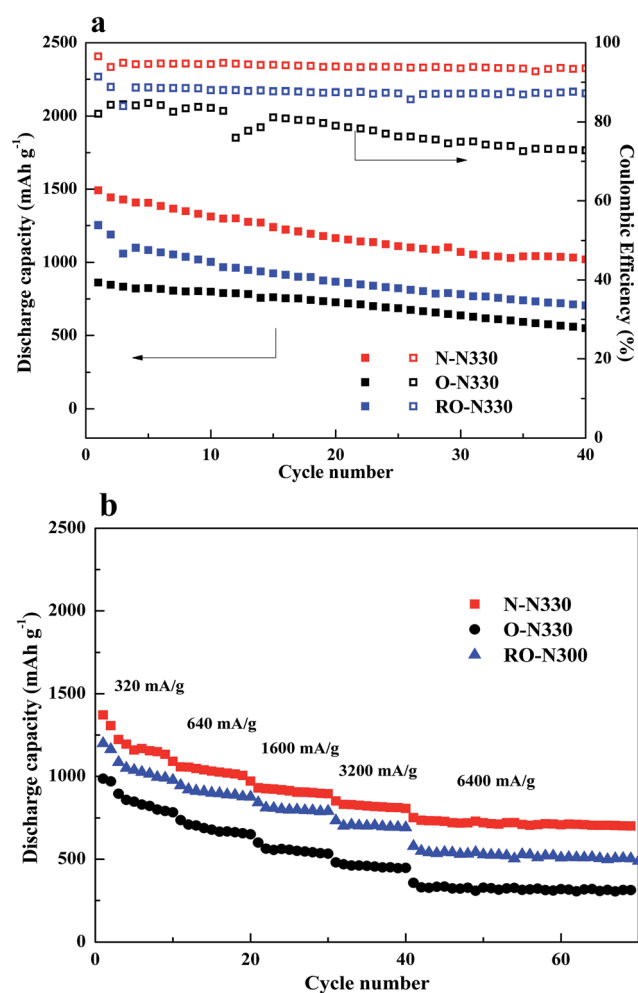| Sample name	Specific surface ($m^2 g^{-1}$)	Pore volume ($cm^3 g^{-1}$)	Mean pore size (nm)
N-N330	1208.98	1.228	4.3
O-N330	1325.45	1.120	3.3
RO-N330	1345.66	1.166	3.5

Fig. 2 Cycle performance at (a) 0.1 C and (b) various current densities of sulfur–carbon black cathodes.
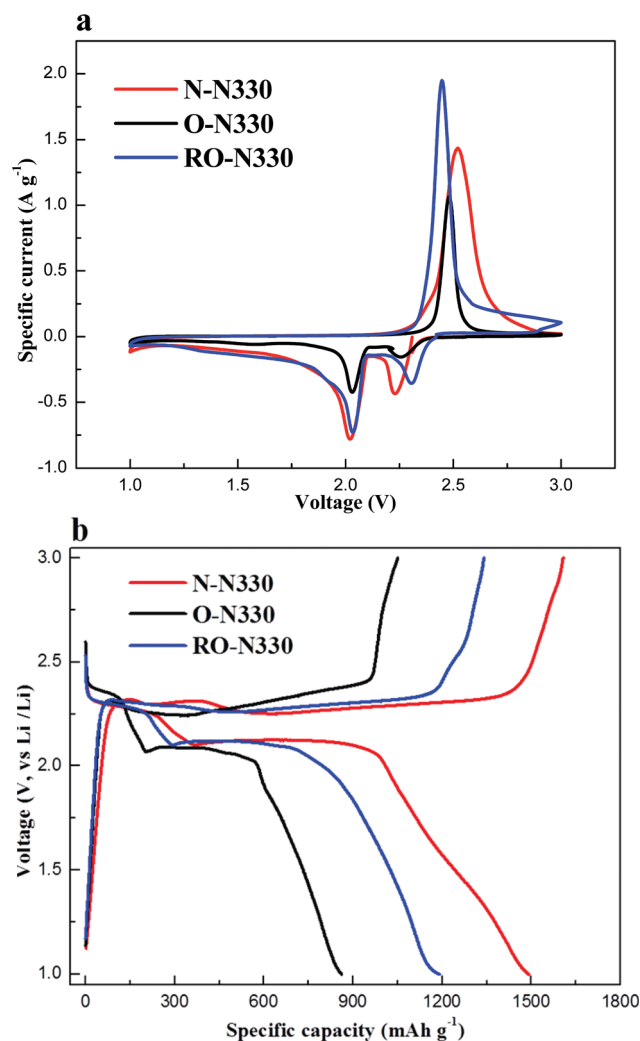

Fig. 3 (a) CV curves and (b) discharge–charge profile of the first redox process of Li–S batteries.

created a system where the role of heteroatoms in Li–S batteries can be isolated and studied.

Cycling performances of sulfur cathodes at 0.1 C (160 mA h g^{-1}) are outlined in Fig. 2a. The three samples present similar tendencies in cycling stability, accounting for the similar physical properties of carbon black. Interestingly, S/N-N330 delivers impressive performance with an initial discharge capacity of about 1490 mA h g^{-1}, indicating very high sulfur utilization (87%). After 40 cycles, the discharge capacity of S/N-N330 maintains about 1020 mA h g^{-1}. Moreover, S/N-N330 exhibits an elevated coulombic efficiency of 93%, confirming a highly reversible Li–S redox reaction. However, S/RO-N330 and S/O-N330 show relatively lower capacities and coulombic efficiencies. Especially, S/O-N330 only presents a capacity of 550 mA h g^{-1} after the 40th discharge cycle. The rate performance is also one of the great concerns on rechargeable batteries. As shown in Fig. 2b, S/N-N330 demonstrates significantly better rate performance compared to S/O-N330 and S/RO-N330, with a capacity of over 700 mA h g^{-1} under 6400 mA g^{-1} after 70 cycles, indicating excellent tolerance to drastic current density alterations during battery cycling.

Detailed analysis of electrochemical reactions was conducted by cyclic voltammetry. Fig. 3a shows the normalized CV

profiles at a scanning rate of 0.1 mV s^{-1}. Two cathodic peaks at 2.3 V and 2.1 V and one anodic peak at 2.5 V are shown in the first sweeping cycle, correlating with discharge–charge potential plateaus displayed in Fig. 3b. The two cathodic peaks are associated with the two-step discharging process, consistent with the prevailing Li–S mechanism.[24–27] During the cathodic process, sulfur firstly reduced into S_8^-, corresponding to the cathodic peak at 2.3 V; then stepwise reduced into low-order polysulfides (S_2^{2-}, S^{2-}), corresponding to the peak at 2.1 V.[28–30] Interestingly, N-N330 performs much lower anodic peak intensity than that of RO-N330 while the two cathodic peak intensities are comparable, implying shuttle effect relief by the N-N330 host. On the other hand, the normalized peak area of
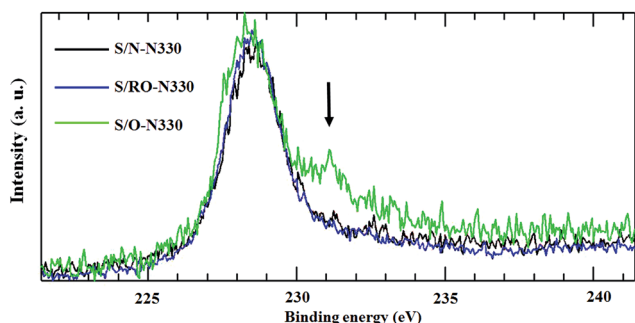

Fig. 6 Raman spectra of as-prepared carbon black samples and the inserted form is the value of I_D/I_G of carbon blacks.

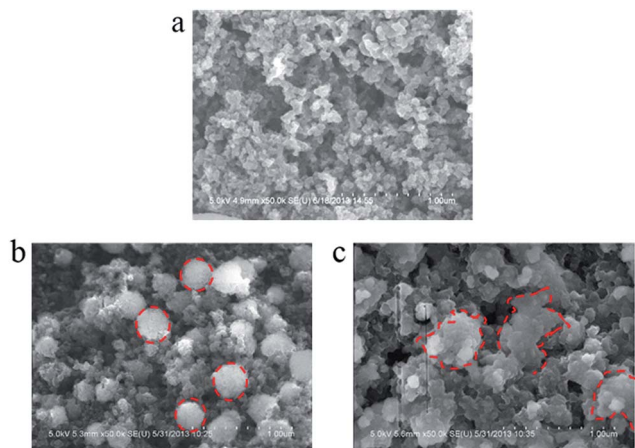Fig. 4 Synchrotron-based S 2s XPS spectra of sulfur−carbon black composites.

Fig. 5 FE-SEM images of electrodes of (a) N-N330, (b) RO-N330, and (c) O-N330 after 30 charge–discharge cycles.
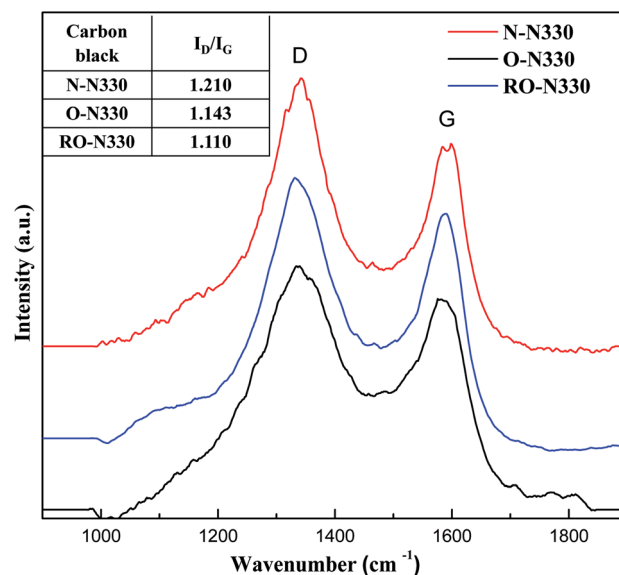

Fig. 7 Synchrotron-based Li 1s XPS spectra of sulfur electrodes after cycling.

This journal is © The Royal Society of Chemistry 2014

J. Mater. Chem. A, 2014, **2**, 12866–12872 | **12869**

S/O-N330 is much smaller than that of the other two samples. This may be due to the limited electrochemical activity and reduced cycling performance. The aforementioned electrochemical performance results highlight the improved performance of N-N330 over O-N330 and RO-N330 samples, with O-N330 demonstrating dramatically reduced performance. The following discussion will elucidate the reason for heteroatom effects on the significant difference of electrochemical performances.

Fig. 4(a) shows the synchrotron-based XPS spectra for the sulfur 2s core level of sulfur–carbon black composites. Interestingly, S/O-N330 shows an additional peak at higher binding energy, indicating that a part of sulfur is oxidized to a higher valence state. This information correlates well with FTIR spectra obtained for S/O-N330 (Fig. S3†), where the presence of S–O bonds is clearly visible. Along with the reduced cycling performance of S/O-N330, these results suggest that an unexpected reaction occurs between sulfur and surface oxygen species to form S–O functional groups. These unwanted side reactions may raise three issues: (1) loss of the active sulfur material during cycling; (2) deterioration of the host conductive carbon material; and (3) elevated irreversible product formation during cell operation.[31–33]

The mechanism of discharge product formation for Li–sulfur batteries is based on the electrical conductivity of the electrode, sorption effects of the carbon host, and reversibility of Li–sulfur reactions.[34,35] As shown in the SEM images, S/N-N330 electrodes maintain their initial morphology, while S/RO-N330 and S/O-N330 electrodes display sphere-like and even aggregating slab-like discharge products deposited on the surface (as outlined in red). This provides strong evidence that the discharge products of S/N-N330 are more uniformly distributed across the substrate surface as a result of nitrogen inclusion (Fig. 5).

Raman spectra of carbon black materials were acquired to determine the graphitic order of carbon followed by NH_3, CO_2 and CO_2/H_2 treatment (Fig. 6). D (1350 cm^{-1}) and G bands (1590 cm^{-1}) are associated with the disordered and graphitic carbon phase, respectively.[36,37] The values of the peak intensity ratio of D and G bands are given in the table inserted in Fig. 6. N-N330 carbon black exhibits a higher I_D/I_G ratio than O-N330 and RO-N330, indicating greater inclusion of defect sites on the surface. It has been confirmed in our previous work that enriched defect sites are favorable to uniform discharge product deposition in Li–air batteries.[38] In our case, the discharge product Li_2S or Li_2S_2 may also be attracted by nitrogen introduced defect sites, leading to uniform discharge product formation.
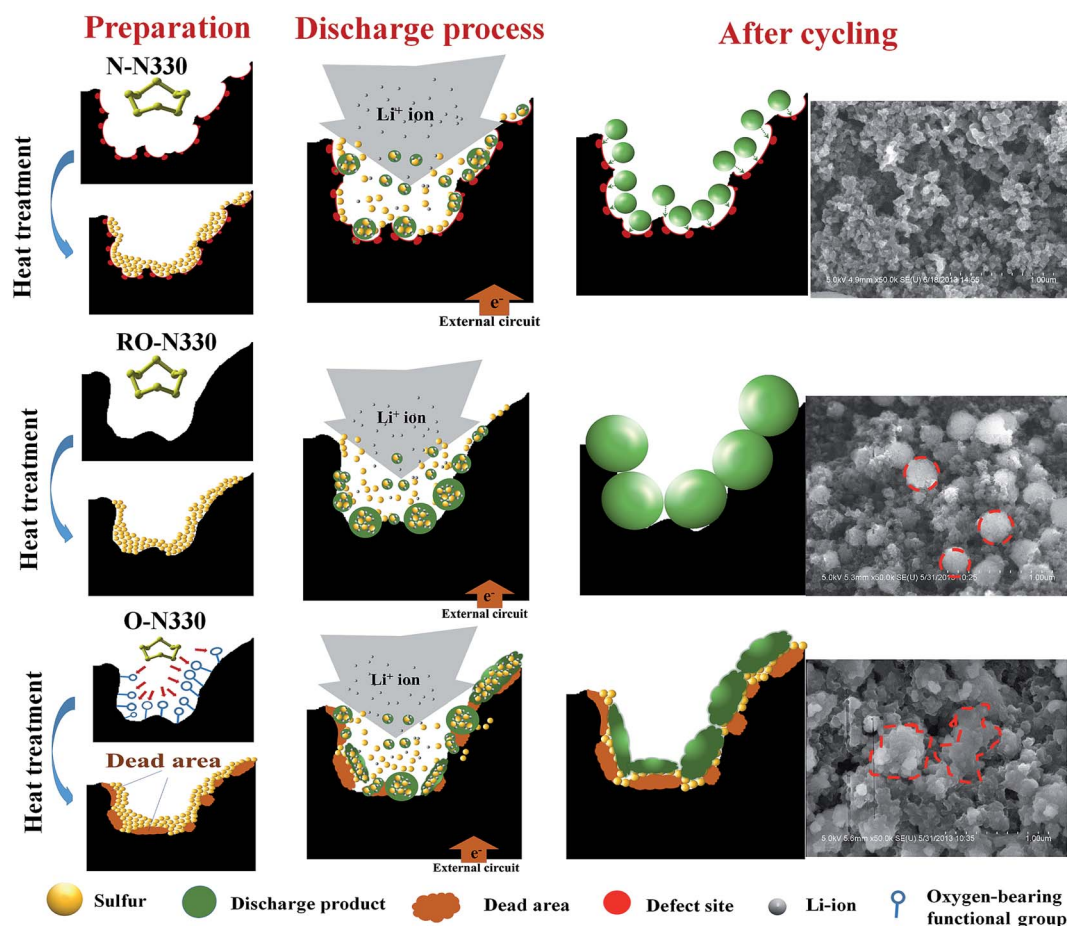

Fig. 8 Schematic diagram showing effects of carbon−heteroatom bonds on sulfur cathodes.

Synchrotron based Li 1s XPS spectra of electrodes after 30 discharge–charge cycles support this explanation, as shown in Fig. 7. Peaks for RO-N330 appear at 55.5 eV which can be attributed to Li 1s electrons in Li_2S.[39,40] Interestingly, peaks for N-N330 showed a slight shift to lower binding energy, corresponding to interactions occurring between Li and nitrogen donated electrons.[41] The interaction between Li and nitrogen is favorable to the uniform dispersed discharge product. It is not very clear why the peak of O-N330 shows a tiny shift to higher binding energy but it may be derived from the formation of $LiSO_x$ or Li_2O_x.[39,42]

Based on the analysis and conclusions drawn above, a schematic diagram of the process for the three sulfur–carbon black cathode systems is outlined in Fig. 8. The enriched defect sites and interaction between lithium and nitrogen of N-N330 result in a uniform distribution of small sized discharge products, thereby improving sulfur utilization and reversibility of Li–S redox reactions, ultimately yielding an improved electrochemical performance. RO-N330 has fewer defects sites, resulting in the formation of larger sized discharge products aggregating on the surface. The O-N330 carbon black undergoes unexpected side reactions with sulfur, leading to reduced conductivity of the electrode and a serious growth aggregation of slab-like discharge products, resulting in a significantly reduced cycling performance.

Conclusions

In order to reveal the influence of heteroatom effects on sulfur cathodes, we developed a series of carbon materials with a similar physical structure. Commercial N330 carbon black was treated with NH_3, CO_2, and CO_2/H_2 to prepare nitrogen-introduced, oxygen-introduced, and bare porous carbon black, respectively. The three sulfur–carbon black composites with different heteroatoms showed varying electrochemical performances. It was found that the enriched defect sites and favorable interaction between N atoms and discharge products result in a uniform distribution of discharge product in the carbon matrix and thereby giving improved electrochemical performance. The O-N330 carbon black underwent unwanted side reactions with sulfur, leading to low sulfur utilization and large slab-like discharge product formation on the electrode. Our work demonstrated that an important correlation exists between carbon–heteroatom bonds and battery performance, and opens a novel direction towards the optimization of carbon host materials used for Li–sulfur batteries.

Acknowledgements

References

1 P. G. Bruce, S. A. Freunberger, L. J. Hardwick and J. M. Tarascon, *Nat. Mater.*, 2012, **11**, 19–29.
2 D. Bresser, S. Passerini and B. Scrosati, *Chem. Commun.*, 2013, **49**, 10545–10562.
3 S. Evers and L. F. Nazar, *Acc. Chem. Res.*, 2013, **46**, 1135–1143.
4 M. K. Song, E. J. Cairns and Y. Zhang, *Nanoscale*, 2013, **5**, 2186–2204.
5 B. Zhang, X. Qin, G. R. Li and X. P. Gao, *Energy Environ. Sci.*, 2010, **3**, 1531–1537.
6 S. H. Chung and A. Manthiram, *Adv. Mater.*, 2014, **26**, 1360–1365.
7 S. Moon, Y. H. Jung, W. K. Jung, D. S. Jung, J. W. Choi and K. Kim do, *Adv. Mater.*, 2013, **25**, 6547–6553.
8 Z. W. Seh, H. Wang, P.-C. Hsu, Q. Zhang, W. Li, G. Zheng, H. b. Yao and Y. Cui, *Energy Environ. Sci.*, 2014, **7**, 672–676.
9 X. Ji, K. T. Lee and L. F. Nazar, *Nat. Mater.*, 2009, **8**, 500–506.
10 L. Ji, M. Rao, H. Zheng, L. Zhang, Y. Li, W. Duan, J. Guo, E. J. Cairns and Y. Zhang, *J. Am. Chem. Soc.*, 2011, **133**, 18522–18525.
11 G. Zheng, Y. Yang, J. J. Cha, S. S. Hong and Y. Cui, *Nano Lett.*, 2011, **11**, 4462–4467.
12 F. Sun, J. Wang, H. Chen, W. Li, W. Qiao, D. Long and L. Ling, *ACS Appl. Mater. Interfaces*, 2013, **5**, 5630–5638.
13 J. Guo, Z. Yang, Y. Yu, H. D. Abruna and L. A. Archer, *J. Am. Chem. Soc.*, 2013, **135**, 763–767.
14 J. Song, T. Xu, M. L. Gordin, P. Zhu, D. Lv, Y.-B. Jiang, Y. Chen, Y. Duan and D. Wang, *Adv. Funct. Mater.*, 2013, **24**, 1243–1250.
15 H. Wang, Y. Yang, Y. Liang, J. T. Robinson, Y. Li, A. Jackson, Y. Cui and H. Dai, *Nano Lett.*, 2011, **11**, 2644–2647.
16 G. Zhou, L. C. Yin, D. W. Wang, L. Li, S. Pei, I. R. Gentle, F. Li and H. M. Cheng, *ACS Nano*, 2013, **7**, 5367–5375.
17 Z. Xiao, Z. Yang, H. Nie, Y. Lu, K. Yang and S. Huang, *J. Mater. Chem. A*, 2014, **2**, 8683–8689.
18 F. Jaouen and J.-P. Dodelet, *J. Phys. Chem. C*, 2007, **111**, 5963–5970.
19 F. Jaouen, A. M. Serventi, M. Lefèvre, J.-P. Dodelet and P. Bertrand, *J. Phys. Chem. C*, 2007, **111**, 5971–5976.
20 Y. M. Yiu, G. Kaur, Q. Xiao and T. K. Sham, *J. Non-Cryst. Solids*, 2013, **364**, 13–19.
21 R. F. Gould, *Coal Science, Advances in Chemistry Series, Foreword*, 1966.
22 M. Seredych and T. J. Bandosz, *Appl. Catal., B*, 2011, **106**, 133–141.
23 F. Lian, F. Huang, W. Chen, B. Xing and L. Zhu, *Environ. Pollut.*, 2011, **159**, 850–857.
24 K. Jeddi, M. Ghaznavi and P. Chen, *J. Mater. Chem. A*, 2013, **1**, 2769.
25 W. Wang, X. Wang, L. Tian, Y. Wang and S. Ye, *J. Mater. Chem. A*, 2013, **2**, 4316–4323.
26 G. Xu, B. Ding, L. Shen, P. Nie, J. Han and X. Zhang, *J. Mater. Chem. A*, 2013, **1**, 4490–4496.
27 H. Xu, Y. Deng, Z. Shi, Y. Qian, Y. Meng and G. Chen, *J. Mater. Chem. A*, 2013, **1**, 15142–15149.

28 G. C. Li, G.-R. Li, S.-H. Ye and X.-P. Gao, *Adv. Energy Mater.*, 2012, **2**, 1238–1245.

29 S. Chen, X. Huang, H. Liu, B. Sun, W. Yeoh, K. Li, J. Zhang and G. Wang, *Adv. Energy Mater.*, 2014, DOI: 10.1002/aenm.201301761.

30 K. Kumaresan, Y. Mikhaylik and R. E. White, *J. Electrochem. Soc.*, 2008, **155**, A576.

31 Y. Diao, K. Xie, S. Xiong and X. Hong, *J. Power Sources*, 2013, **235**, 181–186.

32 S. S. Zhang, D. Foster and J. Read, *J. Power Sources*, 2010, **195**, 3684–3688.

33 D. Dong, Y. Zhang, S. Sutaria, A. Konarov and P. Chen, *PLoS One*, 2013, **8**, e82332.

34 D. W. Wang, G. Zhou, F. Li, K. H. Wu, G. Q. Lu, H. M. Cheng and I. R. Gentle, *Phys. Chem. Chem. Phys.*, 2012, **14**, 8703–8710.

35 C. Zu, Y. Fu and A. Manthiram, *J. Mater. Chem. A*, 2013, **1**, 10362.

36 R. Dillon, J. Woollam and V. Katkanant, *Phys. Rev. B: Condens. Matter Mater. Phys.*, 1984, **29**, 3482–3489.

37 A. Sadezky, H. Muckenhuber, H. Grothe, R. Niessner and U. Pöschl, *Carbon*, 2005, **43**, 1731–1742.

38 Y. Li, X. Li, D. Geng, Y. Tang, R. Li, J.-P. Dodelet, M. Lefèvre and X. Sun, *Carbon*, 2013, **64**, 170–177.

39 D. Aurbach, E. Pollak, R. Elazari, G. Salitra, C. S. Kelley and J. Affinito, *J. Electrochem. Soc.*, 2009, **156**, A694.

40 F. Changming, G. Haichun, H. Yan, C. Zengliang and Z. Yi, *Solid State Ionics*, 1991, **48**, 289–293.

41 A. K. Arof, N. M. Morni and M. A. Yarmo, *Mater. Sci. Eng., B*, 1998, **55**, 130–133.

42 L. Suo, Y. S. Hu, H. Li, M. Armand and L. Chen, *Nat. Commun.*, 2013, **4**, 1481.